Journal of Power Sources 392 (2018) 129–138

Contents lists available at ScienceDirect

Journal of Power Sources

journal homepage: www.elsevier.com/locate/jpowsour

Temperature dependence of corrosion of ferritic stainless steel in dual atmosphere at 600–800 °C

Patrik Alnegren[a,*], Mohammad Sattari[b], Jan-Erik Svensson[a], Jan Froitzheim[a]

[a] Division of Energy and Materials, Department of Chemistry and Chemical Engineering, Chalmers University of Technology, Sweden
[b] Division of Materials Microstructure, Department of Physics, Chalmers University of Technology, Kemivägen 10, 41296, Gothenburg, Sweden

HIGHLIGHTS

- Breakaway corrosion occurs when a steel is exposed to dual environment of air/H_2.
- Passive layers forms on reference samples in air only.
- There is an inverse temperature dependence of the dual atmosphere effect.

ARTICLE INFO

Keywords:
High temperature oxidation
Solid oxide fuel cells
Interconnect
Dual atmosphere
AISI 441
Hydrogen

ABSTRACT

The ferritic stainless steel AISI 441 (EN 1.4509) is exposed for 1000 h to air - 3% H_2O on one side and to Ar - 5% H_2 – 3% H_2O on the other at temperatures 600, 700, and 800 °C. Conditions are chosen to mimic the environment of metallic interconnects in an operating solid oxide fuel cell (SOFC). At 600 °C, ~25 μm thick Fe_2O_3/$(Fe,Cr)_3O_4$ forms on large parts of the air side of the samples. Reference samples exposed to air - 3% H_2O on both sides form thin protective layers of $(Cr,Mn)_3O_4/Cr_2O_3$ at the same temperature. At higher temperatures, 700 and 800 °C, all samples form protective layers of $(Cr,Mn)_3O_4/Cr_2O_3$ regardless of exposure to single or dual atmosphere. It is concluded that corrosion resistance in a dual atmosphere has an inverse dependence on temperature. Different hypotheses for the underlying cause for the dual atmosphere effect are discussed and compared to the experimental data.

1. Introduction

Solid oxide fuel cells (SOFC) are high-efficiency energy conversion devices that, due to their high operating temperature of 500–900 °C, are able to run on a variety of different fuels. These fuels range from hydrogen to hydrocarbon gases, like natural gas and reformate gas. The most common way to build SOFC units is to connect individual planar cells in series to create a fuel cell stack of up to 100 cells, depending on the power requirements. The modular nature of the fuel cell stack makes it a very scalable technology, which allows for designing systems with power capacities ranging from a few hundred watts up to megawatts. The individual fuel cells within a stack are separated by metallic interconnects, which also provide electrical contact between each cell.

Interconnects are generally made of ferritic stainless steels due to their thermal expansion coefficient (TEC), which matches the other cell components, in combination with good formability and electrical conductivity at a reasonable cost. For these steels, corrosion resistance is achieved by the formation of a chromium oxide layer on the steel surface, which acts as a diffusion barrier and slows down the oxidation of the steel part. For interconnects, it is important that the protective chromia layer is well adherent to avoid loss of electrical contact, and that the layer is slow growing since a thicker chromia layer leads to higher ohmic losses [1]. Furthermore, chromium should preferably be oxidized over iron, since iron oxide grows several orders of magnitude faster than chromium oxide and, thus, offers poor corrosion protection. The ability of a steel to form a protective chromia scale is affected by many factors, such as the concentration of Cr in the steel, the alloy microstructure, the surface treatment, and by minor alloying elements [2]. The preferential oxidation of chromium in a stainless steel is also greatly affected by the environment to which it is exposed. For instance, stainless steels in atmospheres with a high steam content are known to be prone to form iron oxide when they would otherwise form protective chromia scales in atmospheres of air at the same temperature [3]. In SOFC stacks the interconnects are exposed to high pO_2 on the oxidizing side and to low pO_2 on the fuel side and conduct electric current in the range of 0.1–1 A cm^{-2}. It has been shown that electric current can

* Corresponding author.
E-mail address: patrik.alnegren@chalmers.se (P. Alnegren).

https://doi.org/10.1016/j.jpowsour.2018.04.088
Received 14 February 2018; Received in revised form 24 April 2018; Accepted 25 April 2018

affect the oxidation of ferritic stainless steels. In general, the oxidation rate is reduced on the cathode side and increased at the anode side [4–6] but accelerated corrosion, with iron nodule formation, on both the anode and the cathode has also been reported [7].

Several researchers have shown, in the context of SOFCs, that when exposed to hydrogen on one side and air on the other side, ferritic stainless steel sheets tend to form more iron oxide on the air side than when only exposed to air or hydrogen atmospheres [8–15]. Similar findings have also been reported in the context of steam and flue gas tubes, in which corrosion was found to be accelerated on the air side of the tubes [16,17]. It should be noted that the magnitude of the reported effects varies significantly between different studies. E.g. Kurokawa et al. [18] and Ardigo et al. [7] do not observe accelerate oxidation under dual atmosphere conditions. This disagreement is probably due to experimental differences, such as hydrogen concentration, pre-treatment of sample as well as alloy composition.

The dual atmosphere effect, i.e. promotion of iron oxide on the air side, is likely caused by the diffusion of hydrogen through the steel substrate, which interferes with the oxidation process on the air side of the sample. It has been shown that hydrogen can diffuse relatively fast through a steel sheet and at 600 °C a permeation rate in the order of mm h^{-1} can be expected [19]. Skilbred and Haugsrud have found increased hydrogen content in the oxide scale of the air side of a dual-atmosphere-exposed ferritic stainless steel at 800 °C [20]. The flux of hydrogen is initially expected to be determined by the steel thickness, but after oxidation and formation of a Cr_2O_3 scale the flux quickly becomes rate limited by the chromia thickness. Kurokawa et al. measured four orders of magnitude lower permeability for hydrogen in the oxide scale formed on Fe16Cr compared to the hydrogen permeability in ferrite at 800 °C [21]. The mechanism for how hydrogen affects the air-side oxide scale is unknown. Yang et al. have suggested altered defect chemistry of the protective chromia scale due to doping with hydrogen, which leads to an increase in metal ion diffusivity [8]. Holcomb et al. have suggested that steam formation within the oxide results in pore formation that offers fast transport of oxygen, which leads to accelerated corrosion [10]. Other findings that might explain the dual atmosphere effect are:

- Increased internal oxidation, which causes the immobilization of Cr and results in the depletion of Cr near the metal oxide [22].
- Formation of hydroxides on oxygen sites in the oxide lattice, which allows for faster oxygen diffusion due to the smaller ionic radius of the hydroxides compared to oxygen ions [23].

Most studies on the oxidation of ferritic steels in dual atmospheres have been carried out at temperatures of around 800 °C. In a previous study, we exposed the ferritic stainless steel AISI 441 to a dual atmosphere at 600 °C and found a strong dual atmosphere effect [14]. Local iron oxide nodules of up to 25 µm thickness were found on the air side of the samples exposed for 1000 h to humid air on one side and to humid hydrogen on the other. In contrast, the samples exposed to humid air on both sides formed protective scales with a thickness in the order of a few hundred nm, consisting of chromia and chromium manganese spinel. The strong dual atmosphere effect at the relatively low temperature of 600 °C led to the suspicion that the dual atmosphere effect might have an inverse relation to temperature, meaning that thicker oxide scales are formed at lower temperatures. Such inverse temperature dependence has been reported for ferritic steels exposed to a single atmosphere of humid hydrogen [24] and when exposed to a flow of humid air [25]. In both studies the authors explained this by a change of the oxidation mechanism. It is suggested that due to an insufficient flux of Cr from the alloy towards the metal/oxide interface the chromia scale growth cannot be maintained and non-protective Fe rich oxide is formed instead. In the paper by Jonsson et al. [25] this transition to a non-protective regime is explained by Cr depletion caused by the formation of gaseous $CrO_2(OH)_2$ in the presence of water vapor (see Equation (1)) [26].

Table 1
Composition in wt% of the specific batch of AISI 441 used in this study, provided by Sandvik Materials Technology.

Material	Fe	Cr	Ni	Mn	Si	Ti	Nb	C	P	S
AISI 441	Bal	17.7	0.19	0.30	0.55	0.15	0.37	0.015	0.027	0.002

$$½Cr_2O_3(s) + ¾O_2(g) + H_2O\,(g) = CrO_2(OH)_2(g) \quad (1)$$

The aim of the current study is to investigate the temperature dependence of the dual atmosphere effect by exposing the ferritic stainless steel AISI 441 at different temperatures, using the same experimental setup and ferritic stainless steel as in the previous study at 600 °C [14].

2. Experimental

Circular specimens with 20 mm diameter were cut from 0.2 mm thick AISI 441 foil and were cleaned with acetone and ethanol in an ultrasonic bath. No further surface treatment was performed on the steel. The surface finish of the steel was bright-annealed with a roughness of 0.1–0.3 µm, according to Sandvik Materials Technology, which provided the material. The composition of the AISI 441 ferritic stainless steel used is given in Table 1. To simulate SOFC stack production, where the stack is usually initially heated to a higher temperature in air, the samples were pre-oxidized at 800 °C in ambient atmosphere for 3 h before exposure to dual atmosphere, and the mass change after pre-oxidation was recorded. The samples were placed in a 253 MA steel holder, based on a design from National Energy Technology Laboratory [10,11,27], which allows for separate control of gas composition, including humidity, and gas flow on each side of the samples. Gold gaskets were used to seal the ferritic stainless steel samples to the holder, and gas tightness was controlled regularly. The humidity level was checked using a chilled mirror humidity sensor (Michelle – Optidew Vision). The sample holder was placed in a horizontal tube furnace (60 mm diameter). A heating/cooling rate of 5 °C min^{-1} was used and the setup was flushed for at least 12 h before heating was initiated. For more details on the experimental setup and sample holder, see Ref. [14].

Duplicate samples were tested in each experiment in which one set of samples was exposed to air on one side and to humid hydrogen on the other side. This will hereinafter be referred to as “dual atmosphere”. Another set of samples was used as references and was exposed to air on both sides, and this will be referred to as “single atmosphere”. The gas flow rate, gas contents, and temperature in the experiments carried out in this study are listed in Table 2. Exposures were conducted at temperatures of 600 °C, 700 °C, and 800 °C in high-flow humid air. A humidity of 3% was used to promote formation of volatile $CrO_2(OH)_2$ [28] and to replicate standard simulated SOFC cathode conditions of our laboratory [29]. The flow rates for the air were chosen to achieve an average flow speed of approximately 27 cm s^{-1} and were calculated from the dimension of the inside and outside (silica tube diameter) of the sample holder. Based on a previous study, this rate should be in a

Table 2
Conditions used in the experiments.

Temp.	Outer gas	Inner gas 1 (dual atmosphere)	Inner gas 2 (single atmosphere)
600 °C	8800 sml min^{-1} air – 3% H_2O	100 sml min^{-1} Ar - 5% H_2 – 3% H_2O	400 sml min^{-1} air – 3% H_2O
600 °C	600 sml min^{-1} air	100 sml min^{-1} Ar - 5% H_2 – 3% H_2O	50 sml min^{-1} air
700 °C	8800 sml min^{-1} air – 3% H_2O	100 sml min^{-1} Ar - 5% H_2 – 3% H_2O	400 sml min^{-1} air – 3% H_2O
800 °C	8800 sml min^{-1} air – 3% H_2O	100 sml min^{-1} Ar - 5% H_2 – 3% H_2O	400 sml min^{-1} air – 3% H_2O

flow regime in which the chromium evaporation rate is kinetically controlled, i.e. independent of flow rate [29]. Another experiment was carried out at 600 °C with lower flows of dry air. The dry experiment was carried out to lower the formation of $CrO_2(OH)_2$. This experiment will be referred to as the "600 °C dry" experiment hereinafter for the purpose of simplicity.

The samples were photographed after exposure with a Canon EOS 1D mk III camera, equipped with a Canon 100 mm f/2.8 macro lens. This was done while the samples were still mounted in the sample holder. Thus, only the sides exposed to air (Outer gas) were photographed. Detailed analyses of the microstructure and chemical composition were performed using a Zeiss LEO ULTRA 55 FE-SEM scanning electron microscope (SEM) and an FEI Titan 80–300 scanning transmission electron microscope (STEM), both equipped with an Oxford Instruments INCA X-Sight energy-dispersive X-ray spectroscopy (EDX) system. Samples for TEM were prepared with focused ion beam (FIB) milling and in-situ lift-out technique in an FEI Versa 3D DualBeam instrument. A Leica EM TIC 3X broad ion beam (BIB) instrument was used to prepare cross sections (in the range of mm) of the samples. All the cross sections were cut perpendicular to the rolling direction of the ferritic stainless steel sheet. It was not possible to record reliable mass gains of the exposed samples using the current experimental method due to damage to the sample during dismounting and interference with the gold seals. Oxide thickness, therefore, was measured in the micrographs of cross sections. On the 600 °C samples, large grains of $(Cr,Mn)_3O_4$ grown on top of a Cr_2O_3 layer resulted in large variations of the total oxide thickness. For this reason, we chose to focus on measuring the oxide thickness of the 700 °C samples, which was done in the following manner: micrographs were obtained at 10 equidistant positions on cross sections of 1–2 mm width, where each micrograph showed 10 μm of the sample along the surface. The total oxide thickness of these micrographs was measured in 10 equidistant positions, totaling 100 measurement points for each sample. The thickness of the oxide on the 600 and 800 °C samples was measured for selected micrographs, with 30–70 measurement points per sample. X-ray diffraction (XRD) was performed on selected samples with a Siemens D5000 diffractometer with a grazing incidence angle of 3°. Due to thin oxides at 600 °C and spalling oxides at 800 °C, in combination with bent samples after dismounting from the sample holder, the 700 °C samples were chosen for X-ray diffraction analysis.

3. Results

The photographs of all air sides of the samples are displayed in Fig. 1. After exposure to single atmosphere at 600 and 700 °C, the surfaces look metallic and shiny, which indicates thin protective oxide layers. The 600 °C samples exposed to humid air have some small, dark-colored nodules, which were identified with SEM/EDX as iron oxide. Our previous findings showed that these iron oxide nodules did not grow after continued exposure beyond 1000 h, meaning that a protective layer of chromia must have formed underneath the nodules [14]. These iron oxide nodules are absent from the samples exposed to single atmosphere and dry air at 600 °C. At 800 °C, some of the oxide spalled off during the cool down of the furnace, which is evident by the exposed, unoxidized bare metal on the edges of the samples. A major difference is seen at 600 °C in a comparison of samples exposed to dual atmosphere and those exposed to single atmosphere. After exposure to dual atmosphere, both with humid and dry air, a large part of the samples surfaces are covered with dark-colored iron oxide. The areas on these samples that are not covered with iron oxide, i.e. the areas with protective oxide, look similar to the surface of the single atmosphere samples. Each microstructure will be discussed in more detail below. At 700 and 800 °C, there are no apparent differences between single and dual atmosphere samples.

The 700 °C samples were analyzed with XRD, and the obtained diffractograms are displayed in Fig. 2. Peak pattern matching of the diffractograms show the presence of both a spinel and a corundum phase. This, in combination with SEM/EDX data (discussed below) indicates that the thin protective oxide layers consist of an inner layer of Cr_2O_3 and an outer layer of $(Cr,Mn)_3O_4$, as is commonly found in chromia-forming steels that contain Mn [30]. Based on previous studies, the oxide layers on 600 °C and 800 °C samples are also expected to be made up of an inner chromia layer and an outer chromium manganese spinel layer [31,32]. Fig. 3 shows SEM micrographs of cross sections of a single atmosphere sample. Duplex layered oxide formation can be seen within the whole tested temperature range in the figure. The $Cr_2O_3/(Cr,Mn)_3O_4$ that formed on all samples is made up by continuous, nano-grained chromia with larger spinel grains on top. Fig. 4 shows air side cross sections of the dual atmosphere samples. The composition and morphology of the oxide layers at 700 and 800 °C are essentially the same as for the single atmosphere samples. The thin and yet protective parts of the oxide at 600 °C are similar to the oxide of the single atmosphere samples. In contrast, the thicker oxides that formed on the air sides of the dual atmosphere samples are made up of an outward-growing layer of iron oxide and an inward-growing layer of chromium-iron oxide. This kind of oxide morphology was also observed by Young et al. on ferritic stainless steels exposed to Ar- 4% H_2 – 20% H_2O at the temperature range of 500–650 °C [24].

The outer layer consists of a hematite layer containing 95 cation% Fe according to SEM/EDX measurements, while the inner layer contains approximately 50-50% Fe-Cr and, consequently, is expected to form a spinel phase [33]. Fig. 5 shows cross sections of the hydrogen sides of the dual atmosphere samples. The oxides on the hydrogen sides are protective with duplex layers of inner chromia and outer chromium manganese spinel, similar to the protective air-side oxides. At 700 and 800 °C more pores are observed within the oxide scale, compared to the air side. This is commonly observed for scales formed in the presence of H_2/H_2O [34].

A TEM micrograph of a cross section from the air-side oxide of a sample exposed to dual atmosphere at 600 °C is shown in Fig. 6. A nodule of thicker iron oxide can be seen in the figure with a surrounding thinner protective oxide. The microstructure, characteristics, and composition of the breakaway oxide were described and discussed more in detail in our previous paper [14]. EDX linescans were done to measure the Cr depletion profile beneath the protective oxide. In scan A, a minimum Cr content of 16.8 atomic% is measured right below the chromia scale, which increases to 18.8 atomic% further into the alloy. In scan B, a larger Cr depletion is observed, with values ranging from 11.7 to 18.2 atomic%. The presence of a silica layer beneath the chromia is also observed.

Fig. 7 shows TEM micrographs of cross sections of the air sides of both the single atmosphere and dual atmosphere samples exposed at 700 °C and EDX linescans through the oxide and into the bulk alloy. These are representative micrographs and linescans chosen from a total of six analyses per sample. For both samples, the top layer spinel phase typically contained 40 cation% Mn, 50 cation% Cr, and 5 cation% Fe, while the bottom layer corundum phase contained 95 cation% Cr and 1–2 cation% Fe. Between the chromia layer and the bulk, there is a thin layer of silica. The 700 °C samples do not show any Cr depletion in the alloy near the oxide. The 800 °C air-side cross sections were also analyzed with SEM/EDX (not shown here) and no difference in the composition of the oxide and the alloy near the oxide is found between single and dual atmosphere samples. The chromia formed on those samples contains 1–2 cationic% Fe and no Cr depletion is seen in the alloy bulk. Continuous silica below the chromia layer is present in the 800 °C samples.

4. Discussion

4.1. Temperature effect

A substantial dual atmosphere effect was observed after exposure at

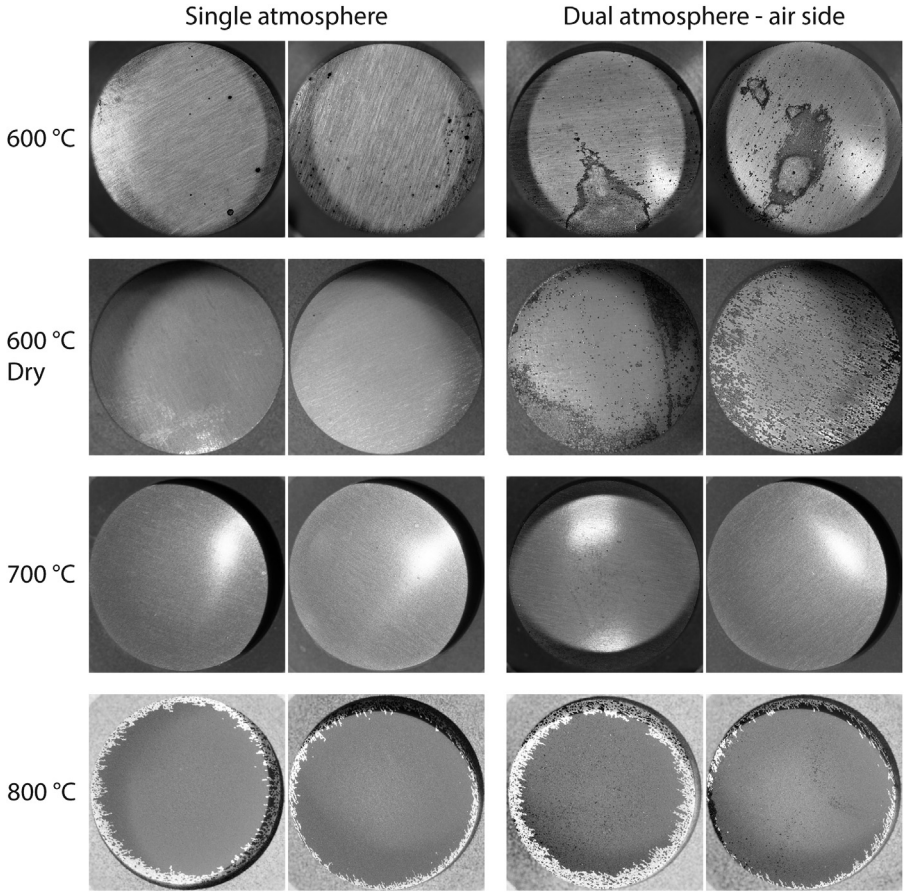

Fig. 1. Photographs of the samples after 1000 h of exposure to dual and single atmosphere at 600, 700 and 800 °C.

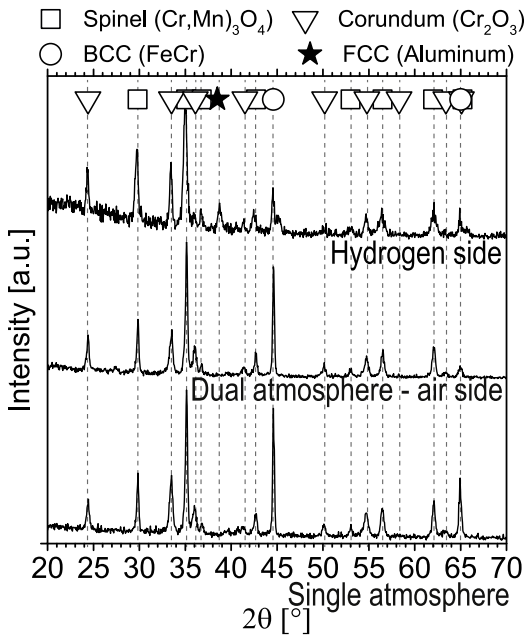

Fig. 2. X-ray diffractograms of the surfaces of samples exposed at 700 °C for 1000 h. The star-shaped data marker represent a peak from aluminum, which originates from the aluminum sample holder.

600 °C, where thick iron nodules formed on the air side of the ferritic stainless steel specimen. It was found that this effect disappeared when the temperature increased and protective layers of Cr_2O_3 with $(Cr,Mn)_3O_4$ on top formed, regardless if the samples had been exposed to a dual or single atmosphere. In order to sustain a protective chromia scale, the consumption of chromium from oxidation cannot exceed the resupply from the bulk. For this reason, a critical concentration of chromium is necessary within the alloy to maintain sufficient chromium flux from the bulk alloy towards the oxide/metal interface. Insufficient chromium bulk diffusivity at lower temperatures has been pointed out as the cause for breakaway corrosion in several studies, e.g. Refs. [24,25]. If the activation energy of the alloy interdiffusion coefficient for Cr is higher than that for Cr consumption from oxidation, a higher concentration of Cr in the steel is required to sustain a protective layer at lower temperatures than at higher ones. The exposure environment can change the apparent activation energy of oxidation. Young et al. have found that the activation energy for oxidation was lower in an Ar - 4% H_2 – 20% H_2O environment (110 kJ mol^{-1}) than in air (179 kJ mol^{-1}). Those authors derived an equation to calculate the critical chromium concentration based on Wagner's expression for parabolic oxidation:

$$\ln N_{Cr,\,crit} = const. + \frac{Q - E_A}{2RT} \quad (2)$$

where $N_{Cr,\,crit}$ is the critical chromium concentration for maintaining a protective chromia scale, Q is the activation energy for the diffusion of chromium in the alloy, and E_A is the activation energy for the parabolic rate constant (k_p). This would lead to a higher critical Cr concentration at a lower temperature if $Q > E_A$. Falk-Windisch et al. have reported that, at 650 °C in high-flow rate air – 3% H_2O, the main contribution to Cr consumption is the formation of volatile chromium oxyhydroxide. Those authors measured an activation energy of 91 kJ mol^{-1} for the Cr volatilization. This led to the hypothesis that the large dual atmosphere effect at a lower temperature might be due to the fact that Cr

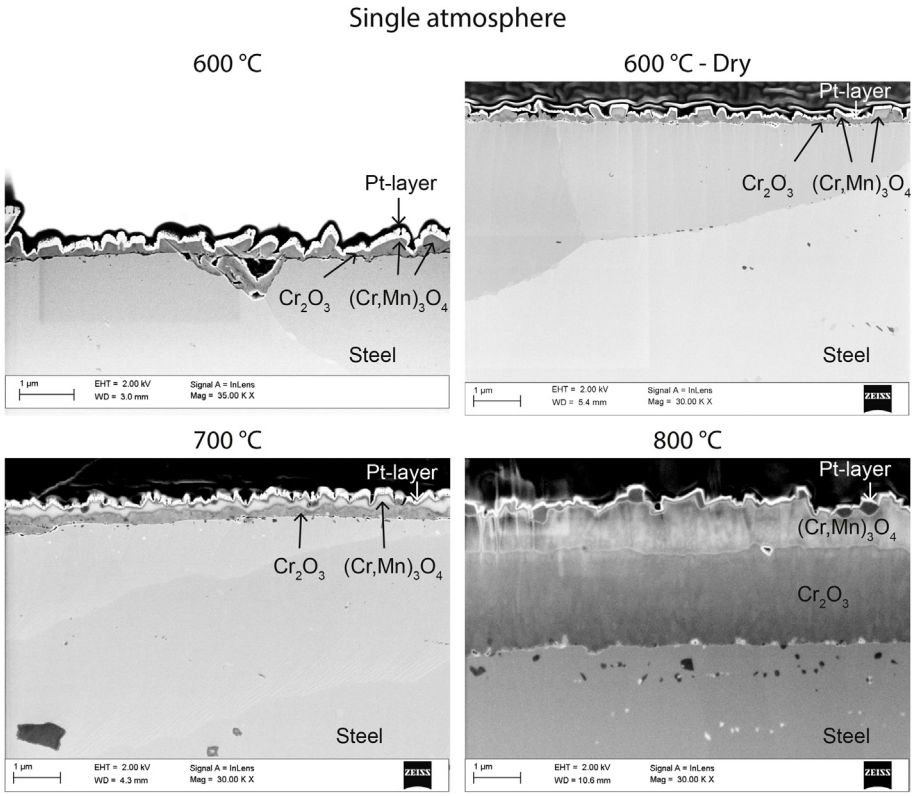

Fig. 3. SEM micrographs of cross sections of oxides on the single atmosphere samples after 1000 h.

evaporation has a lower activation energy than Cr diffusion. However, when Cr evaporation was significantly reduced in the present study by lowering air humidity and the flow rate, we still found a significant dual atmosphere effect at 600 °C. Thus, it seems that Cr volatilization can only play, at the most, a minor role in explaining the inverse temperature effect on the dual atmosphere phenomenon. The measured scale thickness of the areas with protective oxide on the air side of the dual atmosphere and single atmosphere samples did not differ significantly at any temperature. This indicates that the activation energy for oxidation is similar in both cases. However, when the temperature increases, the solubility of hydrogen in ferrite increases [35], but the solubility, or uptake, of hydrogen in chromia decreases [36]. This means that there is the possibility that hydrogen causes more defects in the oxide at lower temperatures, thus increasing the oxidation rate. This will be discussed in more detail in the following section.

4.2. Dual atmosphere effect

4.2.1. Altered oxide scale defect concentration

In a study by Yang et al., a ferritic stainless steel was exposed to dual atmosphere at 800 °C and an iron-rich oxide was formed on the air side of the samples [8]. The authors proposed that increased cation transport due to hydrogen doping of the chromia scale a might be a possible mechanism for the accelerated corrosion. Yang et al. suggested that hydrogen enters the oxide as a proton and donates its electron, or rather forms hydroxide with an effective positive charge. If this effective positive charge is compensated by Cr vacancies, there should be more available sites for cation transport, which would explain the increase in iron content. This is based on the assumption that the chromia scale is a p-type conductor. This model of explanation is supported by the work of Hultquist et al. who have oxidized pure chromium, containing different contents of dissolved hydrogen, in air at 900 °C [37]. The authors found that the oxidation rate increased and that cationic transport increased when the hydrogen content was higher in the chromium samples.

In an electrical conductivity study of chromia, Holt and Kofstad concluded that, at temperatures below 1000 °C, chromia is an extrinsic p-type conductor in a high pO_2 atmosphere [36]. According to those authors, this is likely due to inevitable trace amounts of lower valent dopants. Furthermore, Young and Gerretsen have found that, at lower oxygen pressures, close to the dissociation pressure of chromia, it is an n-type conductor with Cr interstitials as the predominant defects [38]. Galerie et al. performed photoelectrochemical measurements on chromia scales grown on ferritic stainless steel [23]. Those authors also concluded that, in air, the outer part of the oxide was p-type, and the inner part was n-type. When oxidizing the same ferritic stainless steel in steam, only n-type chromia formed. Those authors have suggested that hydrogen must be a donor dopant and forms hydroxides in the lattice. The smaller ionic radius of OH^- compared to O^{2-} has been suggested to lead to faster diffusion of oxygen in chromia, which would account for a faster oxidation rate [23,36]. This would also explain the change towards a more inward-growing oxide on steels exposed to environments with steam and hydrogen. Several studies have shown that chromia-forming alloys have a weak dependence on oxidation rate when the oxygen pressure is varied. This is indicative of a predominantly n-type oxide [39]. If hydrogen enters n-type chromia and forms hydroxide, and also forms Cr vacancies for charge compensation, this will lead to a poorer ionic conductor. Instead, hydrides would have to form for the ionic conductivity to increase in the case of n-type chromia. There is another possibility for hydrogen to enter chromia; Tanaka et al. have performed hydrogen permeation experiments on n-type chromia grown on ferritic stainless steel in an H_2/H_2O environment at 1000 °C [40]. Those authors concluded that hydrogen is uncharged in the chromia lattice and occupies oxygen vacancies.

If the ionic conductivity of the chromia layer increases due to hydrogen doping, it will lead to a faster oxidation rate, which could cause breakaway corrosion if Cr is not supplied fast enough from the alloy. If Cr transport towards the metal/oxide interface is sufficient, the resulting oxide layer should grow thicker than an oxide layer absent of hydrogen doping. Fig. 8 shows graphs of the measured protective oxide

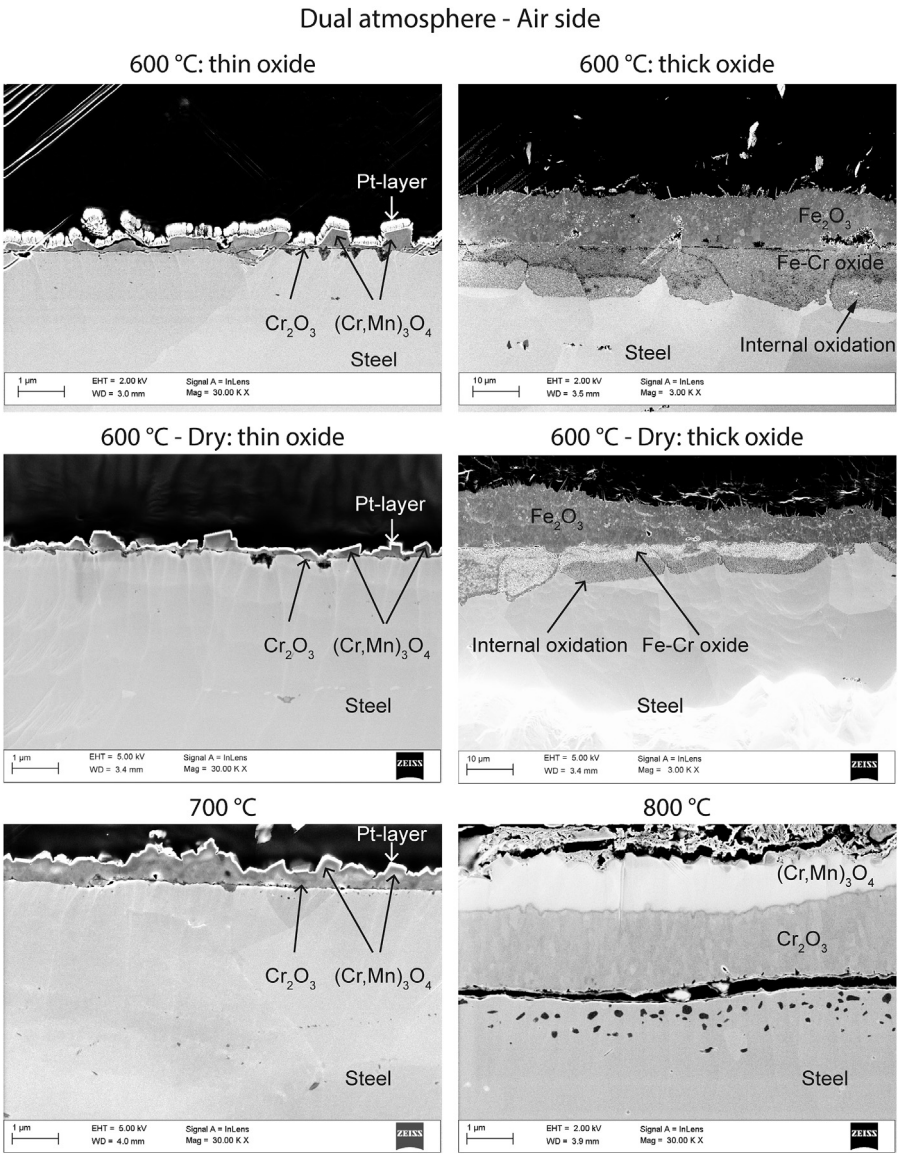

Fig. 4. SEM micrographs of cross sections of the air side oxides on the dual atmosphere samples after 1000 h. For the samples exposed at 600 °C both thin protective oxide and thick breakaway oxide are shown in separate micrographs (note the different magnifications).

thicknesses of the samples after exposure, as well as the calculated oxide thickness after pre-oxidation (based on mass gains and a dense chromia scale). The figure shows that the average thickness at 600 °C was 200 nm, at 700 °C it was 500 nm, and at 800 °C it was 2.7 µm. On the hydrogen side at 700 and 800 °C, the measured oxide thicknesses were slightly lower than on the air sides, while they were similar at 600 °C. The average oxide thickness of samples exposed to 600 °C only increased some tens of nanometers compared to the calculated thickness after pre-oxidation. Overall, there are no significant differences in the measured thicknesses between the airsides of samples exposed to a single or dual atmosphere. Nevertheless, minor differences could still be present but not detected due the amount of variation in the measurements.

Although an effect of hydrogen on the defect chemistry of Cr_2O_3 is undisputed the measured thicknesses of the protective oxides did not differ significantly between dual- and single-atmosphere-exposed samples at any temperature. Thus it is concluded that any potential hydrogen doping does not affect the oxide scale growth rate sufficiently to be the main cause for breakaway corrosion. The EDX data from 700 °C cross sections (Fig. 7) show that the Fe contents in both the spinel and the corundum phases are similar in both single and dual atmospheres. Consequently, the presence of hydrogen in the dual atmosphere samples does not seem to alter the relative diffusivity of Fe and Cr, which otherwise could explain the formation of non-protective hematite.

4.2.2. Oxide cracks from steam formation within the oxide scale

Holcomb et al. have found that 316 L tubes with hydrogen flowing inside formed iron oxide on the outside if exposed to ambient air at 700 °C [10]. Based on thermodynamic calculations on partial pressures of hydrogen and oxygen, those authors suggest that the breakdown of the protective oxide might be caused by steam formation within the air-side oxide scale. However, significant energy would be required in order for steam to form under such confined conditions. Furthermore, hydroxide formation in the chromia scale in the presence of an hydrogen atmosphere has been suggested to cause the oxide to increase in plasticity due to the higher mobility of hydroxides compared to oxygen ions [23,36]. If steam is developed inside the oxide scale it should lead to more porosity. We, however, did not observe more porosity in the protective scales grown in a dual atmosphere than in a single atmosphere at any temperature. The breakaway oxide formed after dual atmosphere exposure at 600 °C contained more pores, but this is common for this rapid mode of oxidation and is more probably a

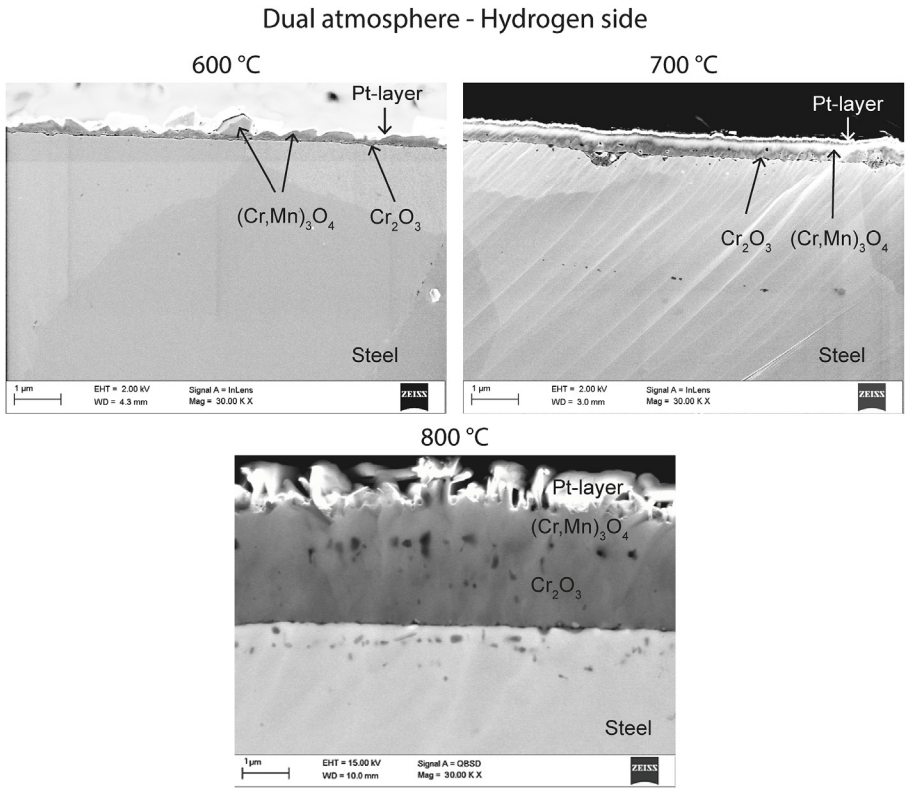

Fig. 5. SEM micrographs of cross sections of the hydrogen side oxides on the dual atmosphere samples after 1000 h.

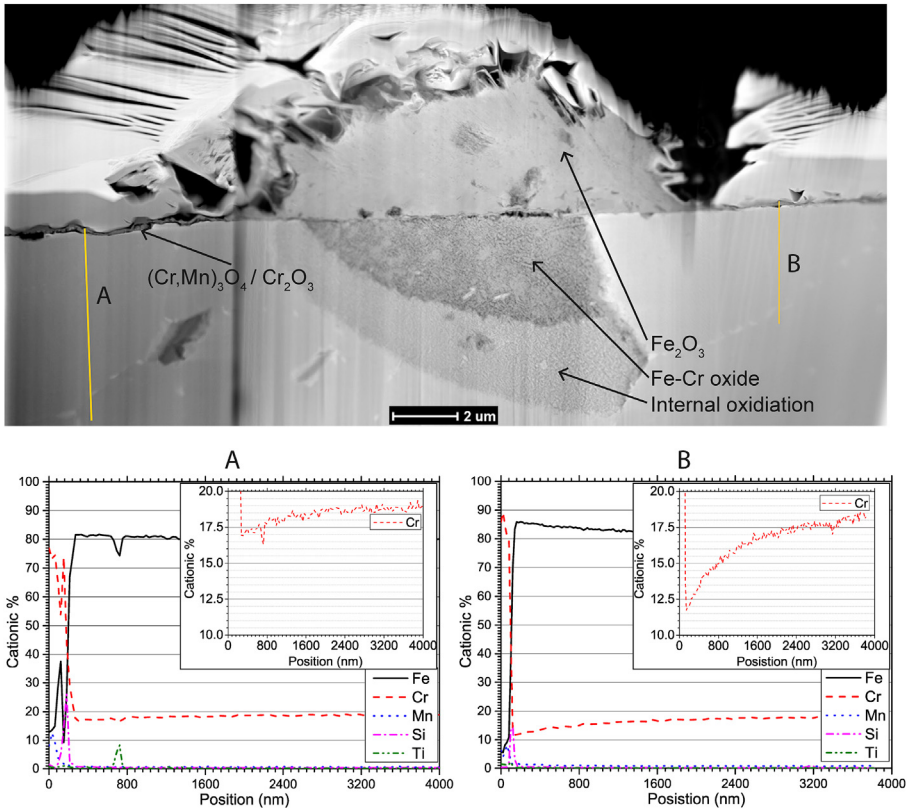

Fig. 6. High angle annular dark filed (HAADF) STEM micrograph of a cross section through an iron oxide nodule on the air side of a sample exposed to dual atmosphere at 600 °C. Compositional data from EDX linescans at positions below protective parts of the oxide is also shown.

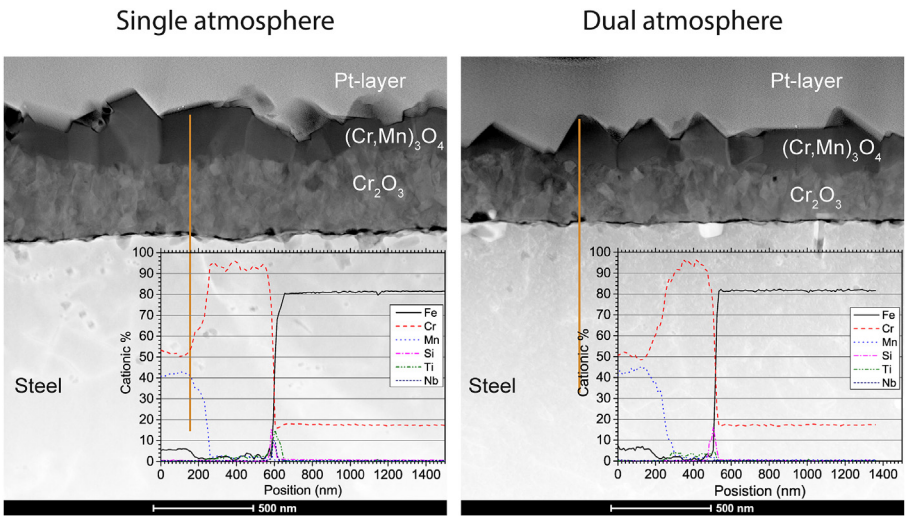

Fig. 7. High angle annular dark filed (HAADF) STEM micrographs of cross sections of air side oxides on samples exposed to single and dual atmosphere at 700 °C for 1000 h. Compositional data from EDX linescans through the oxides is also shown. The micrographs and respective EDX linescans were chosen as representative from a total of six micrographs/EDX scans per sample.

consequence of the breakdown of the protective oxide.

4.2.3. Internal oxidation/reduced chromium activity

A possible cause for breakaway corrosion could be that hydrogen directly, or indirectly, decreases the mobility of Cr in the alloy. The solubility of hydrogen in a Fe-Cr alloy increases with higher contents of Cr [35]. This indicates that a chemical interaction takes place between hydrogen and chromium, which, in turn, could lead to lower Cr activity. However, since the solubility of hydrogen in ferrite is in the range of 100 atomic ppm [41], interaction with hydrogen is expected to have very little effect on Cr activity. Another cause for a reduction in Cr activity could be the formation of the intermetallic Fe-Cr phase, called the σ-phase, which could tie up Cr in the alloy. The Cr concentration required for σ-phase formation decreases with temperature, and the formation of σ-phase has been confirmed for ferritic stainless steels at 650 °C [42]. Although σ-phase formation has, to our knowledge, not been reported for AISI 441, the presence of hydrogen could potentially stabilize σ-phase. Hammer et al. observed increased σ-phase formation in the presence of H_2O [43]. Analyses of a cross section of a dual-atmosphere-exposed sample with SEM/EDX and EBSD maps did not indicate any σ-phase formation after 1000 h at 600 °C.

A decrease in Cr diffusivity in the alloy caused by dissolved hydrogen is not supported in the literature. Cr depletion experiments conducted by Park et al. at 800 °C showed an increase in the Cr diffusion rate when the steel was annealed in hydrogen [44]. Ani et al. have performed Fe-FeCr coupled diffusion experiments in atmospheres with and without hydrogen, which showed no difference in Cr diffusion in the two environments [45]. However, both Park et al. and Ani et al. have claimed that oxygen permeability increases in atmospheres of higher hydrogen pressure. Essuman et al. have also suggested that hydrogen in Fe-Cr alloys increases the diffusion rate of oxygen in the bulk, due to a higher chemical driving force and a larger lattice size [22]. This, in turn, could lead to the internal oxidation of Cr, which would tie up Cr within the bulk. Examination of the cross sections of the parts with protective oxide on the samples exposed at 600 °C (Figs. 3 and 4) showed that there is no difference in the prevalence of internal oxidation between single and dual atmosphere samples. However, if internal oxidation leads to a breakdown of the protective chromia scale, rapid breakaway oxidation would follow, with typical inward-growing and outward-growing phases. This makes the initiation phase difficult to detect. The EDX linescans of the alloy below the protective oxide, in the vicinity of an iron oxide nodule in Fig. 6 show significant depletion of Cr on one side of the nodule. However, no signs of internal oxide near the linescan (Fig. 6B) was detected, which would otherwise explain the lower Cr concentration.

5. Conclusion

A clear effect of exposure to dual atmosphere was found at 600 °C. Samples exposed to dual atmosphere conditions at 600 °C formed thick iron oxide on the air side, while samples exposed in air only formed thin protective oxide scales. The fact that hydrogen affects the oxidation properties on the air side proves that hydrogen diffuses through the oxide on the hydrogen side and through the steel and somehow

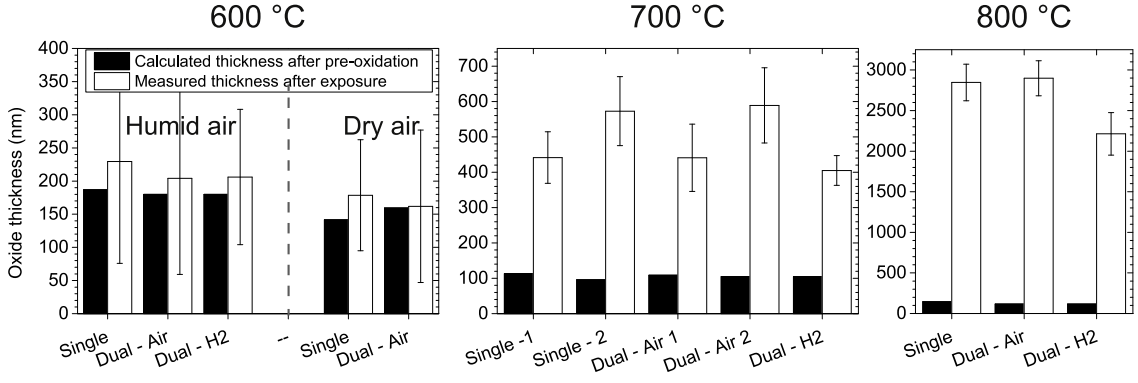

Fig. 8. Oxide thicknesses after pre-oxidation and after 1000 h exposure to all test environments. The oxide thickness after pre-oxidation (filled bars) were calculated from mass gains. The oxide thicknesses after exposure was measured from cross sections and the error bars represent the standard deviation. Duplicate samples were measured for 700 °C samples, indicated by the numbers 1 and 2.

interacts with the oxidation process on the air side in such a way that formation of chromia is inhibited. At 700 and 800 °C protective chromia scales were observed regardless of exposure conditions. This indicates that the negative effect of hydrogen on the protective scale is compensated for by higher Cr bulk diffusivity at higher temperatures. The thickness, microstructure, and composition of the protective layers of $(Cr,Mn)_3O_4/Cr_2O_3$ did not vary significantly between samples exposed to dual and single atmospheres at any temperature. No evidence was found that the scale growth rate of the protective chromia, is substantially affected by hydrogen, e.g. by doping. An effect of hydrogen that promotes the internal oxidization of Cr was discussed, however, not supported by the experimental findings. Cr loss due to volatilization is known to be weakly temperature dependent (i.e. most important at lower temperatures). This matches well with the observed inverse temperature dependence, but the fact that a severe dual atmosphere effect was also observed under “dry” conditions suggests that other factors might be more relevant.

Acknowledgments

The authors are grateful for funding by the Swedish Energy Agency (grant 2015-009652), the FFI program as well as the Swedish High Temperature Corrosion Centre.

Appendix A. Supplementary data

Supplementary data related to this article can be found at http://dx.doi.org/10.1016/j.jpowsour.2018.04.088.

References

[1] H. Falk-Windisch, J. Claquesin, M. Sattari, J.-E. Svensson, J. Froitzheim, Co- and Ce/Co-coated ferritic stainless steel as interconnect material for intermediate temperature solid oxide fuel cells, J. Power Sources 343 (2017) 1–10, http://dx.doi.org/10.1016/j.jpowsour.2017.01.045.

[2] P. Kofstad, High Temperature Corrosion, Elsevier Applied Science Publishers Ltd., New York, 1988.

[3] S.R.J. Saunders, M. Monteiro, F. Rizzo, The oxidation behaviour of metals and alloys at high temperatures in atmospheres containing water vapour: a review, Prog. Mater. Sci. 53 (2008) 775–837, http://dx.doi.org/10.1016/j.pmatsci.2007.11.001.

[4] P. Kodjamanova, Q. Fu, L. Gautier, Electric current effects on the corrosion behaviour of high chromium ferritic steels, Oxid. Met 79 (2012) 53–64, http://dx.doi.org/10.1007/s11085-012-9325-3.

[5] K. Kawamura, T. Nitobe, H. Kurokawa, M. Ueda, T. Maruyama, Effect of electric current on growth of oxide scale on Fe-25Cr alloy for SOFC interconnect at 1073 K, J. Electrochem. Soc. 159 (2012) B259–B264, http://dx.doi.org/10.1149/2.036203jes.

[6] J. Ryter, R. Amendola, M. McCleary, W.-J. Shong, C.-K. Liu, R. Spotorno, et al., Effect of electrical current on the oxidation behavior of electroless nickel-plated ferritic stainless steel in solid oxide fuel cell operating conditions, Int. J. Hydrogen Energy 43 (2018) 426–434, http://dx.doi.org/10.1016/j.ijhydene.2017.11.055.

[7] M.R. Ardigo, I. Popa, L. Combemale, S. Chevalier, F. Herbst, P. Girardon, Dual atmosphere study of the K41X stainless steel for interconnect application in high temperature water vapour electrolysis, Int. J. Hydrogen Energy (2015), http://dx.doi.org/10.1016/j.ijhydene.2015.01.116.

[8] Z. Yang, M.S. Walker, P. Singh, J.W. Stevenson, T. Norby, Oxidation behavior of ferritic stainless steels under SOFC interconnect exposure conditions, J. Electrochem. Soc. 151 (2004), http://dx.doi.org/10.1149/1.1810393 B669.

[9] Z. Yang, G. Xia, P. Singh, J.W. Stevenson, Effects of water vapor on oxidation behavior of ferritic stainless steels under solid oxide fuel cell interconnect exposure conditions, Solid State Ionics 176 (2005) 1495–1503, http://dx.doi.org/10.1016/j.ssi.2005.03.019.

[10] G.R. Holcomb, M. Ziomek-Moroz, S.D. Cramer, B.S. Covino, S.J. Bullard, Dual-environment effects on the oxidation of metallic interconnects, J. Mater. Eng. Perform. 15 (2006) 404–409, http://dx.doi.org/10.1361/105994906X117198.

[11] J. Rufner, Oxidation behavior of stainless steel 430 and 441 at 800°C in single (air/air) and dual atmosphere (air/hydrogen) exposures, Int. J. Hydrogen Energy 33 (2008) 1392–1398, http://dx.doi.org/10.1016/j.ijhydene.2007.12.067.

[12] A.W. Bredvei Skilbred, R. Haugsrud, The effect of dual atmosphere conditions on the corrosion of Sandvik Sanergy HT, Int. J. Hydrogen Energy 37 (2012) 8095–8101, http://dx.doi.org/10.1016/j.ijhydene.2011.10.096.

[13] R. Amendola, P. Gannon, B. Ellingwood, K. Hoyt, P. Piccardo, P. Genocchio, Oxidation behavior of coated and preoxidized ferritic steel in single and dual atmosphere exposures at 800°C, Surf. Coating. Technol. 206 (2012) 2173–2180, http://dx.doi.org/10.1016/j.surfcoat.2011.09.054.

[14] P. Alnegren, M. Sattari, J.-E. Svensson, J. Froitzheim, Severe dual atmosphere effect at 600 °C for stainless steel 441, J. Power Sources 301 (2016) 170–178, http://dx.doi.org/10.1016/j.jpowsour.2015.10.001.

[15] J. Li, D. Yan, Y. Gong, Y. Jiang, J. Li, J. Pu, et al., Investigation of anomalous oxidation behavior of SUS430 alloy in solid oxide fuel cell dual atmosphere, J. Electrochem. Soc. 164 (2017) C945–C951, http://dx.doi.org/10.1149/2.0251714jes.

[16] K. Nakagawa, Y. Matsunaga, T. Yanagisawa, Corrosion Behavior of Ferritic Steels on the Air Sides of Boiler Tubes in a Steam/Air Dual Environment † vol. 18, (2001), pp. 51–56.

[17] D. Huenert, W. Schulz, A. Kranzmann, Corrosion behavior of ferritic and martensitic power plant steels under conditions of dual atmospheres, Corrosion 66 (2010), http://dx.doi.org/10.5006/1.3524836.

[18] H. Kurokawa, Oxidation behavior of Fe–16Cr alloy interconnect for SOFC under hydrogen potential gradient, Solid State Ionics 168 (2004) 13–21, http://dx.doi.org/10.1016/j.ssi.2004.02.008.

[19] S.K. Yen, Critical hydrogen concentration for the brittle fracture of AISI 430 stainless steel, J. Electrochem. Soc. 143 (1996) 2736, http://dx.doi.org/10.1149/1.1837100.

[20] A.W. Bredvei Skilbred, R. Haugsrud, The effect of dual atmosphere conditions on the corrosion of Sandvik Sanergy HT, Int. J. Hydrogen Energy 37 (2012) 8095–8101, http://dx.doi.org/10.1016/j.ijhydene.2011.10.096.

[21] H. Kurokawa, Y. Oyama, K. Kawamura, T. Maruyama, Hydrogen permeation through Fe-16Cr alloy interconnect in atmosphere simulating SOFC at 1073 K, J. Electrochem. Soc. 151 (2004), http://dx.doi.org/10.1149/1.1767349 A1264.

[22] E. Essuman, G.H. Meier, J. Zurek, M. Hänsel, W.J. Quadakkers, The effect of water vapor on selective oxidation of Fe-Cr alloys, Oxid. Met 69 (2008) 143–162, http://dx.doi.org/10.1007/s11085-007-9090-x.

[23] A. Galerie, J.P. Petit, Y. Wouters, J. Mougin, A. Srisrual, P.Y. Hou, Water vapour effects on the oxidation of chromia-forming alloys, Mater. Sci. Forum 696 (2011) 200–205, http://dx.doi.org/10.4028/ www.scientific.net/MSF.696.200.

[24] D.J. Young, J. Zurek, L. Singheiser, W.J. Quadakkers, Temperature dependence of oxide scale formation on high-Cr ferritic steels in Ar–H2–H2O, Corrosion Sci. 53 (2011) 2131–2141, http://dx.doi.org/10.1016/j.corsci.2011.02.031.

[25] T. Jonsson, S. Canovic, F. Liu, H. Asteman, J.-E. Svensson, L.-G. Johansson, et al., Microstructural investigation of the effect of water vapour on the oxidation of alloy 353 MA in oxygen at 700 and 900°C, Mater. A. T. High. Temp. 22 (2005) 231–243, http://dx.doi.org/10.3184/096034005782744461.

[26] B.B. Ebbinghaus, Thermodynamics of gas phase chromium species: the chromium oxides, the chromium oxyhydroxides, and volatility calculations in waste incineration processes, Combust. Flame 93 (1993) 119–137, http://dx.doi.org/10.1016/0010-2180(93)90087-J.

[27] P. Gannon, R. Amendola, High-temperature, dual-atmosphere corrosion of solid-oxide fuel cell interconnects, JOM (J. Occup. Med.) 64 (2012) 1470–1476, http://dx.doi.org/10.1007/s11837-012-0473-3.

[28] E.J. Opila, D.L. Myers, N.S. Jacobson, I.M.B. Nielsen, D.F. Johnson, J.K. Olminsky, et al., Theoretical and experimental investigation of the thermochemistry of CrO2(OH)2(g), J. Phys. Chem. 111 (2007) 1971–1980, http://dx.doi.org/10.1021/jp0647380.

[29] J. Froitzheim, H. Ravash, E. Larsson, L.G. Johansson, J.E. Svensson, Investigation of chromium volatilization from FeCr interconnects by a denuder technique, J. Electrochem. Soc. 157 (2010), http://dx.doi.org/10.1149/1.3462987 B1295.

[30] W.J. Quadakkers, J. Piron-Abellan, V. Shemet, L. Singheiser, Metallic interconnectors for solid oxide fuel cells – a review, Mater. A. T. High. Temp. 20 (2003) 115–127, http://dx.doi.org/10.3184/096034003782749071.

[31] J.G. Grolig, J. Froitzheim, J.-E. Svensson, Coated stainless steel 441 as interconnect material for solid oxide fuel cells: oxidation performance and chromium evaporation, J. Power Sources 248 (2014) 1007–1013, http://dx.doi.org/10.1016/j.jpowsour.2013.08.089.

[32] H. Falk-Windisch, J.E. Svensson, J. Froitzheim, The effect of temperature on chromium vaporization and oxide scale growth on interconnect steels for solid oxide fuel cells, J. Power Sources 287 (2015) 25–35, http://dx.doi.org/10.1016/j.jpowsour.2015.04.040.

[33] F. Liu, J.E. Tang, T. Jonsson, S. Canovic, K. Segerdahl, J.-E. Svensson, et al., Microstructural investigation of protective and non-protective oxides on 11% chromium steel, Oxid. Met 66 (2006) 295–319, http://dx.doi.org/10.1007/s11085-006-9035-9.

[34] W.J. Quadakkers, J. Żurek, Oxidation in steam and steam/hydrogen environments, Shreir's Corros, fourth ed., Elsevier, 2010, pp. 407–456, , http://dx.doi.org/10.1016/B978-044452787-5.00022-6.

[35] D.M. Coldwell, R.B. McLellan, Thermodynamic properties of Fe-Cr-H ternary solid solutions, Acta Metall. 23 (1975) 57–61, http://dx.doi.org/10.1016/0001-6160(75)90069-3.

[36] A. Holt, P. Kofstad, Electrical conductivity and defect structure of Cr2O3. II. Reduced temperatures (< ~1000°C), Solid State Ionics 69 (1994) 137–143, http://dx.doi.org/10.1016/0167-2738(94)90402-2.

[37] G. Hultquist, B. Tveten, E. Hörnlund, Hydrogen in chromium: influence on the high-temperature oxidation kinetics in H2O, oxide-growth mechanisms, and scale adherence, Oxid. Met 54 (2000) 1–10, http://dx.doi.org/10.1023/A:1004610626903.

[38] E.W.A. Young, J.H. Gerretsen, J.H. Wit, The oxygen partial pressure dependence of the defect structure of chromium(Ill)oxide, J. Electrochem. Soc. 134 (1987) 2257–2260.

[39] P. Alnegren, M. Sattari, J. Froitzheim, J.-E. Svensson, Degradation of ferritic stainless steels under conditions used for solid oxide fuel cells and electrolyzers at varying oxygen pressures, Corrosion Sci. 110 (2016), http://dx.doi.org/10.1016/j.corsci.2016.04.030.

[40] M. Tanaka, M. Ueda, K. Kawamura, T. Maruyama, Hydrogen permeability through

n-type Cr_2O_3 scale at 1273 K under the oxygen activities of 1.6×10^{-18} – 1.0×10^{-16}, ISIJ Int. 51 (2011) 638–644, http://dx.doi.org/10.2355/isijinternational.51.638.
[41] A. San Martin, F.D. Manchester, The Fe-H (Iron-Hydrogen) system, Bull. Alloy Phase Diagrams 11 (1990) 173–184.
[42] L. Niewolak, L. Garcia-Fresnillo, G.H. Meier, W.J. Quadakkers, Sigma-phase formation in high chromium ferritic steels at 650°C, J. Alloy. Comp. 638 (2015) 405–418, http://dx.doi.org/10.1016/j.jallcom.2015.03.076.
[43] J.E. Hammer, S.J. Laney, R.W. Jackson, K. Coyne, F.S. Pettit, G.H. Meier, The oxidation of ferritic stainless steels in simulated solid-oxide fuel-cell atmospheres, Oxid. Met 67 (2007) 1–38, http://dx.doi.org/10.1007/s11085-006-9041-y.
[44] E. Park, B. Hüning, M. Spiegel, Evolution of near-surface concentration profiles of Cr during annealing of Fe–15Cr polycrystalline alloy, Appl. Surf. Sci. 249 (2005) 127–138, http://dx.doi.org/10.1016/j.apsusc.2004.11.078.
[45] M.H. Bin Ani, T. Kodama, M. Ueda, K. Kawamura, T. Maruyama, The effect of water vapor on high temperature oxidation of Fe-Cr alloys at 1073 K, Mater. Trans. 50 (2009) 2656–2663, http://dx.doi.org/10.2320/matertrans.M2009212.